EurJIC
European Journal of Inorganic Chemistry

Chemistry Europe
European Chemical Societies Publishing

Accepted Article

Title: Structural changes in five-coordinate bromido-bis(o-iminobenzo-semiquinonato)iron(III) complex: spin-crossover or ligand-metal antiferromagnetic interactions?

Authors: Valery G Vlasenko, Alexander A Guda, Andrey G Starikov, Maxim G. Chegerev, Alexander V. Piskunov, Irina V. Ershova, Alexander L. Trigub, Andrei A. Tereshchenko, Yurii V. Rusalev, Stanislav P. Kubrin, and Alexander V Soldatov

To be cited as: *Eur. J. Inorg. Chem.* 10.1002/ejic.202001033

Link to VoR: https://doi.org/10.1002/ejic.202001033

WILEY-VCH

10.1002/ejic.202001033

WILEY-VCH

Structural changes in five-coordinate bromido-bis(o-iminobenzo-semiquinonato)iron(III) complex: spin-crossover or ligand-metal antiferromagnetic interactions?

Valery G. Vlasenko,*[a] Alexander A. Guda,*[b] Andrey G. Starikov,[c] Maxim G. Chegerev,[c] Alexander V. Piskunov,[d] Irina V. Ershova,[d] Alexander L. Trigub,[e] Andrei A. Tereshchenko,[b] Yurii V. Rusalev,[b] Stanislav P. Kubrin,[a] Alexander V. Soldatov[b]

[a] Dr. V.G. Vlasenko, Dr. S.P. Kubrin
Research Institute of Physics
Southern Federal University
194 Stachki Ave., Rostov-on-Don 344090, Russia
E-mail: vgvlasenko@sfedu.ru
https://sfedu.ru/en/person/vgvlasenko

[b] Dr. A.A. Guda, A.A. Tereshchenko, Y.V. Rusalev, Prof. A.V. Soldatov
The Smart Materials Research Institute
Southern Federal University
178/24 A. Sladkova street, Rostov-on-Don 344090, Russia
E-mail: guda@sfedu.ru
https://sfedu.ru/en/person/guda

[c] Dr. A.G. Starikov, Dr. M.G. Chegerev,
Institute of Physical and Organic Chemistry
Southern Federal University
194/2 Stachki Ave., Rostov-on-Don 344090, Russia

[d] Prof. A.V. Piskunov, Dr. I.V. Ershova
G. A. Razuvaev Institute of Organometallic Chemistry
Russian Academy of Sciences
49 Tropinina Str., Nizhny Novgorod 603950, Russia

[e] Dr. A.L. Trigub
National Research Center "Kurchatov Institute"
1 pl. Academician Kurchatov, Moscow 123182, Russia

Supporting information for this article is given via a link at the end of the document.

Abstract: Spin-crossover metal complexes represent important building blocks for a future generation of electronic and optical devices. Pentacoordinated o-iminosemiquinonate iron(III) complexes are able to demonstrate spin transitions between high spin (HS) and intermediate spin (IS) states under the influence of temperature or irradiation. Studied (^{Me}imSQ)$_2$FeBr sample showed a broad magnetic transition in the temperature region from 30 K to 300 K. Remarkably that observed behavior of magnetization can be interpreted with two controversial models. In the first model, the values of the effective magnetic moment at low temperature and high temperature can be assigned to the IS and HS magnetic moment of ferric ion coupled antiferromagnetically to radical anion ligands. In the second model, the metal spin on metal center remains IS in the whole temperature interval, while the mutual orientation of three magnetic moments in the molecule undergo changes due to exchange interactions. In this work we apply density functional theory and X-ray absorption spectroscopy to unravel the origin of magnetic properties of the complex. Temperature-induced changes of interatomic distances in the first coordination sphere support the second model. Such comprehensive analysis of the magnetic properties makes it possible to shed light on the nature of spin transitions in complexes of transition metals with open-shell ligands, which are often complicated by strong exchange interactions.

Introduction

Metal complexes with redox-active ligands (o-benzoquinones, o-iminobenzoquinones, diimines) is one of the promising and intensively developing fields of modern organometallic and coordination chemistry. This fact is caused by the unique ability of redox-active ligands to change reversibly its oxidation state being connected to metal center [1-7].

Complexes of transition elements with such type ligands are important objects from the fundamental and applied points of view. Detailed investigation of magnetic properties, electrochemical and spectroscopic features allowed ones to discover such unique phenomena as redox-isomerism (or valence-tautomerism) [3, 8-15], photo and termomechanical effects [16, 17]. Moreover, o-benzoquinone and o-iminobenzoquinone complexes were found to demonstrate a spin-crossover effect [18-23] and different types of inter- or intramolecular magnetic exchange interactions [18-21, 24, 25]. The application of radical-ionic ligands as spin labels in metal complexes allows one to examine their composition, structure and dynamic processes by means of electron paramagnetic resonance spectroscopy [26-28].

On the other hand, redox ligands can be used as reservoirs of electrons for bond-making and bond-breaking reactions. They also able to support multi-electron transformations required to promote atom and group-transfer reactions. This approach is among the modern concepts in the field of catalysis, when metal complexes with redox-active ligands are used for activation of organic molecules [29-33].

Redox-active paramagnetic ligands are gaining increasing interest due to their promising role in molecular magnetism [2, 9,

34-36]. Since o-iminosemiquinones contain an unpaired electron, they can be considered as magnetic centers. Thus, coordination and organometallic compounds constructed as a unique combination of open-shell p-radical ligands and paramagnetic transition metal ions were found to be promising candidates for polyspin systems [4, 7, 21].

Valence-tautomerism (VT) and and spin-crossover (SCO) represent the most efficient and studied processes driving the changes of magnetic properties of transition metal complexes. These phenomena have potential application in molecular electronics involving sensors, switches, memory and other devices, thus making this field relevant to many different areas, ranging from chemistry to solid-state physics [3, 37-42]. It was found that o-iminosemiquinonate iron(III) complexes are able to demonstrate spin transitions between different spin states. For example, hexacoordinated tris-o-iminosemiquinonates $(imSQ)_3Fe$ [21], (where imSQ = radical-anionic o-iminosemiquinone) undergoes a spin-crossover between S_{Fe} = 5/2 → 1/2. In contrast SCO transition between high-spin HS (S_{Fe} = 5/2) and intermediate-spin IS (S_{Fe} = 3/2) is observed for ferric pentacordinated $(imSQ)_2FeHal$ [19, 20] (Hal = halogen atom). In both cases spin-transitions are complicated with strong intramolecular magnetic interactions, which results in changes of the ground states of molecules [43].

Herein we address the local atomic structure around Fe ion and report a combined X-ray spectroscopic investigations temperature induced structural changes in pentacoordinated ferric bis-o-iminosemiquinonate complex containing halogen substituent - $(^{Me}imSQ)_2FeBr$. This complex was recently synthesized in the series of $(^{Me}imSQ)_2FeX$ (X = Cl, Br, I, N_3, NCO) and was discussed as having a spin-crossover behavior [44]. However unusual behaviour of magnetization upon cooling could be alternatively described within the model of exchange coupled trimer (S_1 = 3/2 – spin of Fe(III) ion and $S_2 = S_3$ = 1/2 – spins of radical anion ligands) i.e. when metal is always in intermediate spin state. Mössbauer analysis could not resolve transition between two isolated HS and IS phase in contrast to the related $(^{MeO}imSQ)_2FeCl$ [20] but demonstrated a continuous variation of isomeric shift and quadrupole splitting across all temperature range. Therefore, the question about the magnetic interactions in the complex at different temperatures is open. The purpose of this work is to gain insight about structural changes in the $(^{Me}imSQ)_2FeBr$ complex by X-ray absorption spectroscopy and theoretical DFT modelling to verify which mechanism is realized: spin crossover or strong mutual reorientation of spin magnetic moments on ligands and metal center.

Results and Discussion

Complex of iron(III) $(^{Me}imSQ)_2FeBr$ based on 4,6-di-*tert*-butyl-*N*-(2,6-dimethyl-phenyl)-*o*-aminophenol has been prepared as described previously [20, 44]. Figure 1a shows the schematic structure of the complex.

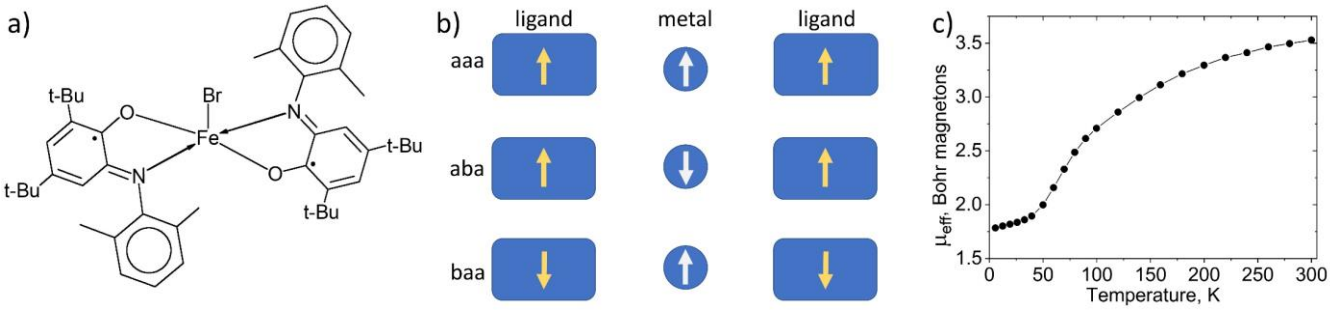

Figure 1. a) Scheme of the ferric complex $(^{Me}imSQ)_2FeBr$ and b) three possible configurations of magnetic moments on metal center and ligands, named as *aaa, aba* and *baa* according to the mutual orientation of spins. c) Temperature dependence of the effective magnetic moment of the complex [44].

Temperature dependence of the effective magnetic moment for the $(^{Me}imSQ)_2FeBr$ is shown in Figure 1c and has a different behaviour from other penta-coordinated ferric complexes $(imSQ^{Me})_2FeX$ with X = Cl, I, N_3 or NCO obtained earlier [44]. On the one hand, saturated values of the magnetic moment at low 10 K (1.75 μB) and high 300 K (3.5 μB) temperatures can be interpreted as a spin-crossover transition between intermediate (S_{Fe}=3/2) and high (S_{Fe}=5/2) spin states on Fe^{3+} ion with antiferromagnetically coupled radical-anion ligands (*aba* configuration in figure 1b for both HS and IS). However, another interpretation is also possible. The temperature behaviour of the magnetization curve can be successfully fitted with effective Hamiltonian model based on constant S_{Fe} = 3/2 spin on Fe ion and strong exchange coupling between two spins S_1=S_2=1/2 on radical-anion ligands [44]. Therefore, experimentally observed variations of the effective magnetic moment between 1.75 μB and 3.5 μB are interpreted as temperature induced variation between fractions of *aaa, aba* and *baa* configurations without spin crossover on the metal center. The two hypotheses are addressed further with X-ray absorption spectroscopy analysis and DFT simulations.

Figure 2 shows experimental Fe K-edge XANES for $(^{Me}imSQ)_2FeBr$ measured in the 30-300 K temperature range. Difference spectra are calculated with respect to the spectrum measured at lowest temperature and indicate prominent changes upon cooling. We observed no shift of the absorption edge therefore oxidation state of Fe remains constant. The series of XANES spectra were further decomposed into two components using principal component analysis (PCA) [46]. The concentrations of the components and spectra itself were

determined using physical constraints: spectra should be normalized, the values of concentrations should be positive, initial and final spectra were considered as a pure state of the complex. As follows from the concentration dependence of the low temperature and high-temperature components on temperature (figure 2b), the phase ratio of both components continuously changes and temperature $T_{1/2}$ is about 110 K. The spectra of pure components are further compared with theoretical spectra for DFT-optimized structural models.

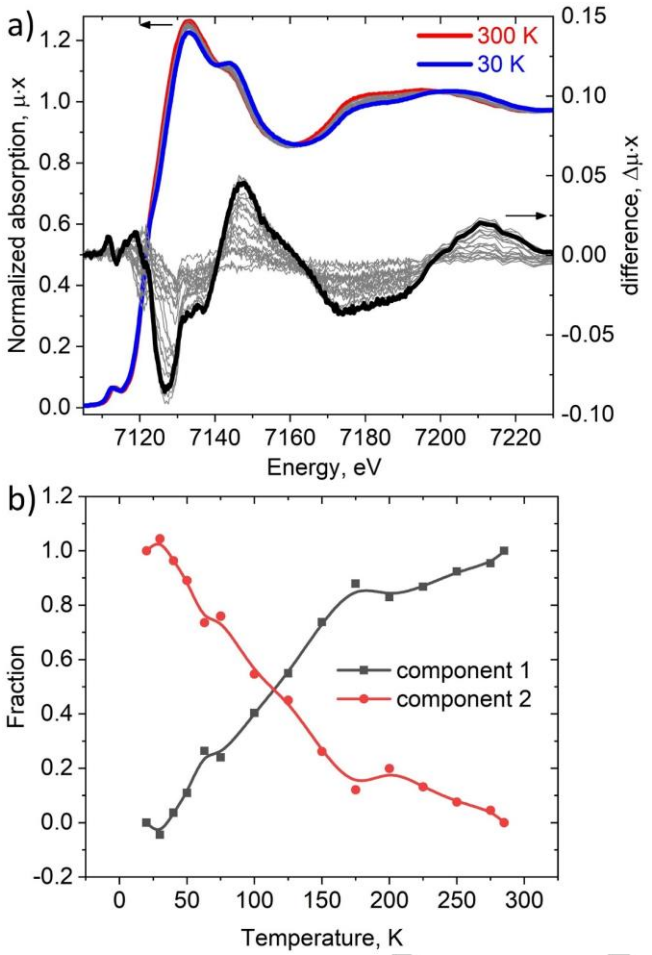

Figure 2. (a) Temperature dependence of normalized Fe K-edge XANES for (^{Me}imSQ)$_2$FeBr in the temperature range 30-300K. Difference spectra (black lines) are calculated with respect to the spectrum measured at lowest temperature. (b) The concentrations of the high-temperature (black) and low-temperature (red) components obtained during PCA analysis as a function of temperature.

XANES spectra of Fe(III) ions in two different spin states HS (S_{Fe} = 5/2) and IS (S_{Fe} = 3/2) and different orientation of spins on metal and ligands (see figure 1b for notations) were calculated by finite difference method.

Figure 3 shows a comparison of the experimental absorption spectra on Fe K-edge of the (^{Me}imSQ)$_2$FeBr complex at temperatures of 30 and 300 K with the theoretical ones. As could be seen in fig. 2, the experimental absorption spectra of (^{Me}imSQ)$_2$FeBr at temperatures of 30 and 300 K are in good agreement with the calculated absorption spectra for DFT structures of IS state of the complex in *aaa* and *aba* configurations. In the case of HS-IS transition (two bottom curves), the amplitude of the theoretical difference is almost 2 times higher than the experimental one. This may indicate the fact that a certain part (around 50%) of the Fe(III) ions does not participate in the HS-IS transition. However, this fact is not supported by single-crystal X-ray diffraction analysis [44] and Mossbauer fits which indicate a fraction of inactive phase less than 10%.

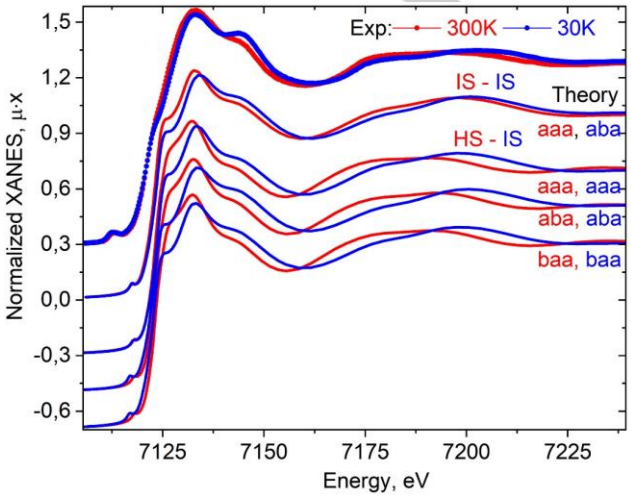

Figure 3. Comparison of experimental spectra on Fe K-edge (^{Me}imSQ)$_2$FeBr at temperatures of 30 and 300 K (solid blue and red lines, respectively) with theoretical ones for IS and HS states and different mutual orientation of spins on metal and ligands (see the Fig. 1).

Figure 4 shows the thermal dependence of the parameters of the (^{Me}imSQ)$_2$FeBr Mössbauer spectrum [44]. The Mössbauer spectrum of (^{Me}imSQ)$_2$FeBr at 14 K has the form of a doublet with isomer shift parameters δ = 0.25 mm/s and quadrupole splitting ΔE_Q,= 2.56 mm/s, characteristic of the intermediate spin (S_{Fe} = 3/2) of Fe(III) ions [19], the values of which gradually change upon heating to room temperature and reach δ = 0.33 mm/s and ΔE_Q = 1.12 mm/s.

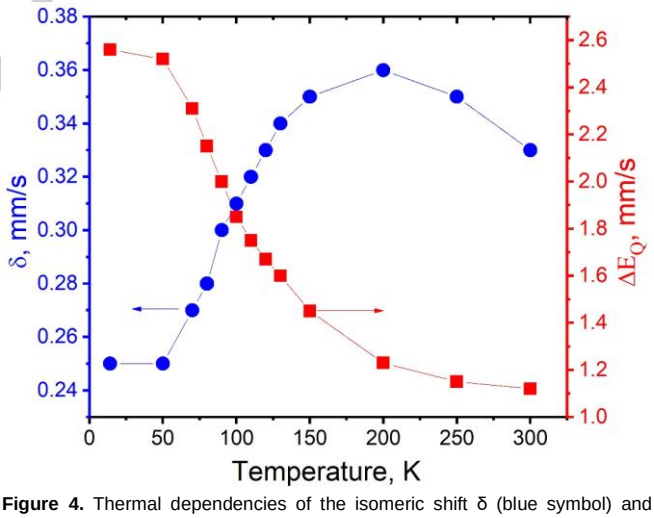

Figure 4. Thermal dependencies of the isomeric shift δ (blue symbol) and quadrupole splitting ΔE_Q (red symbol) of the Mössbauer spectra of a sample of the (^{Me}imSQ)$_2$FeBr complex.

The latter are characteristic for Fe(III) ions with larger distances in the first coordination shell, e.g. for HS state S_{Fe} = 5/2 [47]. The conclusion about spin-crossover from Mössbauer spectra is complicated by the fact that (^{Me}imSQ)$_2$FeBr complex has only a single quadrupole doublet, the parameters of which gradually change with temperature. While for classical SCO behavior two

quadrupole doublets, corresponding to a mixture of different polymorphs of the complex with different spin states of the Fe(III) ion are observed. The absence of the pair of dublets upon transition in Mössbauer spectra is due to the high frequency of the change in spin orientation. If the times of mutual spin transformations are longer than the characteristic time of Mössbauer spectroscopy 10^{-6}-10^{-8} s, then instead of two localized spin states of Fe^{3+}, a doublet with intermediate values of the parameters δ and ΔE_Q is observed [48].

A detailed analysis of the changes in the parameters of the local atomic structure as a function of temperature for (^{Me}imSQ)$_2$FeBr was further determined by calculating the EXAFS Fe K-absorption edges of this compound. FT of (^{Me}imSQ)$_2$FeBr (figure 5) consists of two main well-resolved peaks at r = 1.55 Å and r = 2.05-2.07 Å, the latter has a noticeable shoulder at 2.30-2.40 Å. With decreasing temperature, the amplitude of the first peak changes slightly, while the amplitude of the second peak noticeably increases (by ca. 30%). A qualitative analysis of the composition of the coordination spheres (CSs) was obtained from the analysis of EXAFS Fe K-edges of absorption using the wavelet transformation (WT) [49]. It is known that light atoms C, O, N most efficiently scatter low-energy photoelectrons with small wave vectors *k* (scattering maximum at k = 5–6 Å^{-1}), while for heavier atoms the scattering maximum shifts toward large *k*. The EXAFS WT-map visualizes the pattern of scattering by atoms both in spatial *r*-coordinates and in the coordinates of wavevectors *k*, which allows separating the contributions to scattering from atoms of various types, located, for example, at the same distance from the absorbing center.

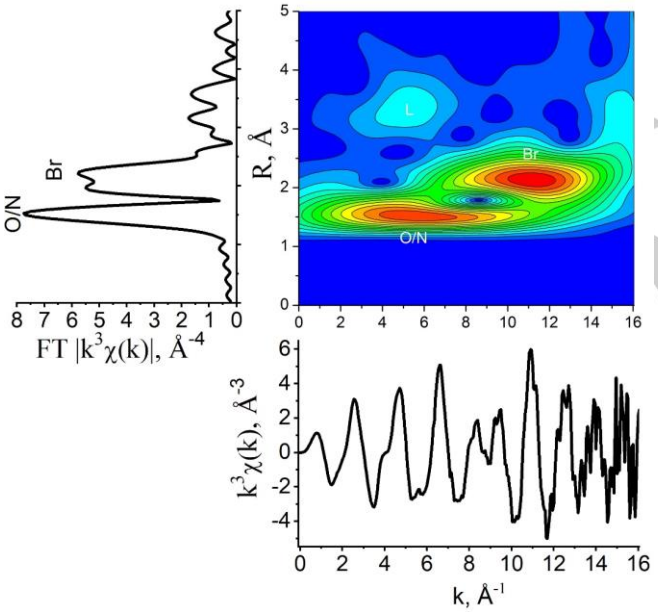

Figure 5. Fe *K*-edge EXAFS signal χ^3(k) (bottom panel), MFT EXAFS (left panel) and Morlet WT EXAFS (central panel) for (^{Me}imSQ)$_2$FeBr at 40 K.

As can be seen in figure 5, EXAFS WT map for (^{Me}imSQ)$_2$FeBr at 40 K has a scattering maximum with coordinates $k \approx 5$ Å^{-1} and r = 1.55 Å^{-1}, clearly indicating that the nearest CS consists of N/O atoms forming the terminal environment of iron ions. For CS with radius *r* = 2.05–2.07 Å, there are two maxima on the WT map with different coordinates in the space of wavevectors. Following the expected (^{Me}imSQ)$_2$FeBr molecular structure, for small $k \approx 5$–6 Å^{-1}, scattering occurs on "light" carbon atoms of the ligands, whereas for large $k \approx 11$ Å^{-1}, scattering occurs on the axial bromine atom. The maxima at large values of $r \approx 3.5$ Å and small $k \approx 5$ Å^{-1} correspond to a scattering of photoelectrons by distant CSs consisting of carbon atoms of bis-o-iminobenzosemiquinone ligands.

The quantitative characteristics of the local atomic environment of iron ions in (^{Me}imSQ)$_2$FeBr at various temperatures were found from the analysis of EXAFS Fe K-edges of these compounds. We performed a three-sphere approximation of the experimental spectra and evaluated the temperature dependences of the Fe – N, Fe – O, and Fe – Br distances. As can be seen in figure 6, over the entire temperature range from 300 to 30 K for the (^{Me}imSQ)$_2$FeBr complex, a gradual decrease in the Fe-N and Fe – O distances occurs, which agrees with gradual changes of quadrupole splitting in Mössbauer spectra and temperature dependences of the effective magnetic moment (μ_{eff}) of (^{Me}imSQ)$_2$FeBr [44]. It should be noted that the Fe-Br distance varies little over the entire temperature range, indicating that the apical bromine atom does not participate in the structural rearrangement during the crossover.

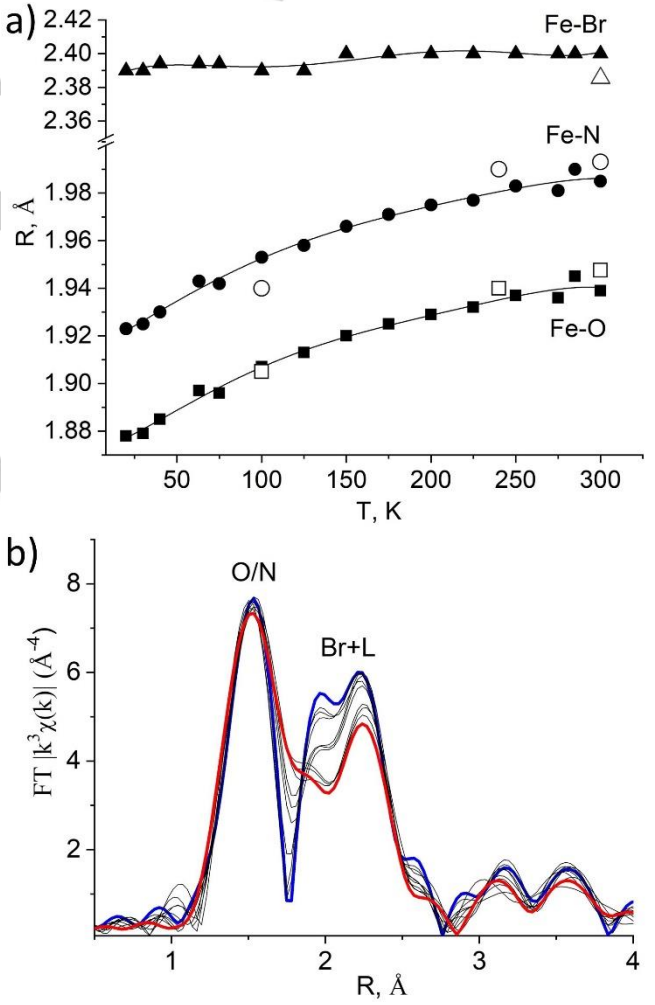

Figure 6. Change in bond distances (a) and MFT EXAFS (b) for (^{Me}imSQ)$_2$FeBr in the temperature range 30-300 K. XRD single crystal data are shown by open symbols.

Table 1. DFT optimized structural parameters of the complex for different orientations of spins of the metal center and ligands. For *baa* state, the two Fe-N distances are not equal and reported with a slash.

	distances	R, Å (HS)			R, Å (IS)		
		aaa	***baa***	***aba***	***aaa***	***baa***	***aba***
TPSSh	Fe-O	2.00	2.00	2.00	1.91	1.91\1.88	1.88
	Fe-N	2.10	2.07	2.05	1.99	1.99\1.92	1.92
	NFeN\OFeO			133\160	150\164	148\164	148\166
B3LYP*	Fe-O	2.01	2.02	2.01	1.92	1.92\1.90	1.89
	Fe-N	2.11	2.12	2.07	2.01	2.01\1.94	1.94
	NFeN\OFeO			133\160	147\164	146\164	147\165
B3LYP*+D3BJ	Fe-O	2.02	2.02	2.01	1.91	1.91\1.90	1.90
	Fe-N	2.06	2.07	2.03	1.97	1.98\1.93	1.93
	NFeN\OFeO			125\159	150\163	145\163	146\164

The values of Fe – N, Fe – O, and Fe – Br bond distances obtained from EXAFS data at various temperatures are in good agreement with the data of XRD analysis for (^{Me}imSQ)$_2$FeBr [44, 45]. Although the distances from XRD were obtained only at three temperatures of 100, 240, and 293 K, an increase in the Fe – O distances in the coordination center from 1.9009(19), 1.9052(19) Å (100 K) to 1.944(2), 1.948(2) Å (293 K) and Fe-N distances from 1.940(2), 1.940(2) Å (100 K) to 1.993(3), 2.003(3) Å (293 K), respectively. It is clearly seen that the absolute values of the Fe – N and Fe – O distances at the corresponding temperature points coincide well (figure 6 open circles). The values of Fe-Br obtained from XRD of the distances of 2.3816(6) Å (100 K) and 2.3755(7) Å (293 K) also confirm our conclusion, obtained from the EXAFS analysis, that they remain constant over the entire temperature range.

Table 1 summarizes the bond length and angles obtained from DFT calculations. As follows from EXAFS analysis average Fe-L (L=O/N) distance changes by 0.06 Å. Assuming the spin-crossover effect between aba configurations the average Fe-L distance changes by 0.12 Å in TPSSh and B3LYP* approximations that is twice larger than observed in the experiment. Addition of dispersion interactions slightly reduces the variation of the distance to 0.11 Å which is anyway too big. On the other hand, the variation of similar distances in IS spin state reaches 0.05 Å for TPSSh and B3LYP* and only 0.03 Å with dispersion interactions included.

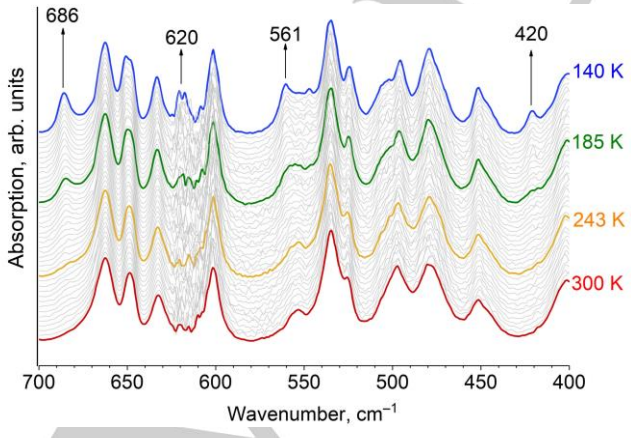

Figure 7. FTIR spectra of (^{Me}imSQ)$_2$FeBr at 140-300 K (region 700-400 cm^{-1}).

The changes in bond length affect the values of the force constants for interatomic interactions. We recorded FTIR spectra (Fig. S1 and S2 Supporting Information) and Figure 7 shows the region from 400 to 700 cm^{-1}, where the strongest changes were observed. The changes include both a variation in the intensity of absorption bands and their position. Bands at 686, 620, 561, and 420 cm^{-1} could be distinguished, the integral intensity of which increases significantly when the sample is cooled. According to DFT calculations, the absorbance in the region of 650–700 cm^{-1} is associated with complex planar deformation of chelate fragments and six-membered rings annelated to them. Other peaks are related to the symmetric and antisymmetric stretching Fe-L vibrations.

It should be noted, that similar possibility of coexistence of exchange magnetic interactions and spin-crossover phenomena (or valence-tautomerism) were found in non-heme iron-nitrosyl complexes. Due to redox-activity of NO substituent different bonding modes between metal center and ligand are possible, which characterized by variety of oxidation and spin states inside the system. Nevertheless, as it was shown that using of combination of XAS, Mossbauer and IR spectroscopy along with DFT calculations allow ones to make unequivocally conclusions about redox-states of Fe and NO moieties in molecule. [50]

Conclusion

We have investigated the local atomic structure of (^{Me}imSQ)$_2$FeBr complex by X-ray absorption and Mössbauer spectroscopy in the wide temperature range. According to the EXAFS analysis, the Fe-O and Fe-N distance increase monotonically across the whole interval 30-300K. The distances obtained from EXAFS are in a good agreement with single-crystal XRD data at corresponding temperatures. Using wavelet analysis, we identified heavy Br atom in the second coordination shell and proved that Fe-Br distance remains almost unchanged upon cooling. The continuous variation of Fe-O and Fe-N distances correlates with observed changes in the variation of quadrupole splitting of a paramagnetic doublet in Mössbauer spectrum and temperature dependence of magnetization. Based on DFT simulations for three possible mutual spin orientations on metal center and ligands, we have evaluated the structure of each state in high spin and intermediate spin states on Fe, i.e. six possible geometries. Theoretical calculations indicate that upon spin-crossover

the difference of Fe-Ligand distances in the first coordination sphere equals 0.12 Å that is twice larger than observed in the experiment. In contrast, the contraction of distances in the IS state for *aaa*, *aba* and *baa* spin orientation configurations is comparable or slightly smaller to the experimentally observed changes. This allows us to conclude that five-coordinated ferric (^{Me}imSQ)$_2$FeBr complex undergoes structural changes upon cooling which can be better described based on strong exchange interactions between spins on metal center and o-iminosemiquinone ligands. The change of spin orientations in *aaa*, *aba* and *baa* configurations within IS the spin state of Fe induce significant structural deformations in the first coordination sphere which can explain experimental FTIR, Mössbauer and XAS data.

Thus, the combination of spectral and theoretical methods allowed us to study the unusual spin rearrangements in the pentacoordinated bis-iminosemiquinone iron(III) complex in details. Such integrated approach can be further extended to a wide range of transition metal complexes with variable magnetic properties.

Experimental Section

X-ray absorption spectroscopy: The temperature dependence Fe *K*-edge XAFS spectra for the complex (^{Me}imSQ)$_2$FeBr were recorded at the "Structural Materials Science" beamline of the Kurchatov Synchrotron Radiation Source (Moscow, Russia), with the storage ring operating at an electron energy of 2.5 GeV and current of 100-120 mA. An Si(111) double-crystal monochromator was used for an energy scan. All data were measured in transmission mode in the temperature range 14-300 K. The thickness *d* of the sample was chosen to satisfy the condition $\mu d \approx 2.0$ for the absorption above the edge and $\Delta\mu d \approx 1$ for the edge jump. EXAFS data $\chi_{exp}(k)$ were analyzed using the IFEFFIT data analysis package [51]. EXAFS data reduction used standard procedures for the pre-edge subtraction and spline background removal. The radial pair distribution functions around the Fe ions were obtained by the Fourier transformation (FT) of the k^3-weighted EXAFS functions $\chi_{exp}(k)$ over the ranges of photoelectron wave numbers k =2.4–13.0 Å^{-1}. The structural parameters, including interatomic distances (R_i), coordination numbers (N_i) and the distance mean-square deviations from thermal motion and static disorder of the absorbing and scattering atoms, also known as Debye-Waller factors (σ^2), were found by the non-linear fit of theoretical spectra to experimental ones. The experimental data were simulated using the theoretical photoelectron mean free path λ(k), amplitude $F_i(k)$ and phase functions $\Psi_i(k)$ (formula 1) calculated using the program FEFF7 [52] and the crystallographic structure for (^{Me}imSQ)$_2$FeBr [45].

$$\chi(k) = S_0^2 \sum_{i=1}^{n} \frac{N_i}{R_i^2} \frac{F_i(k)}{k} e^{-\frac{2R_i}{\lambda(k)}} e^{-2\sigma_i^2 k^2} \sin\left(2kR_i + \Psi_i(k)\right) \quad (1)$$

The amplitude reduction factor S_0^2 was found equal to 0.9 in all cases. The accuracy of the fits was estimated by the standard mean-square deviation criterion.

XANES analysis: Fe K-edge XANES spectra for DFT optimized structures were calculated by means of full-potential finite difference method, implemented in the FDMNES code [53]. The finite difference grid with 0.2 Å interpoint distance was constructed inside a sphere with 6 Å radius around absorbing Fe atom. Theoretical spectra were further convoluted to account for the corehole lifetime broadening and instrumental energy resolution (arctangent function was used to model the energy dependence of the Lorentzian width).

Fourier Transform Infrared Spectroscopy (FTIR): Before the measurement, 5 mg of (^{Me}imSQ)$_2$FeBr was mixed with 10 mg of KBr and thoroughly homogenized in an agate mortar. The resulted mixture was placed in the Praying Mantis Low-Temperature Reaction Chamber (Harrick Scientific Products Inc, New York, USA) installed in the Vertex 70 (Bruker, Billerica, MA, USA) spectrometer equipped with deuterated triglycine sulfate (DTGS) detector. Samples were cooled down under the air atmosphere inside the reaction chamber. The latter was equipped with KBr windows heated by circulating water to prevent frost formation. The FTIR spectra were collected during the whole cooling procedure using the DRIFT technique in the range from 5000 cm^{-1} to 400 cm^{-1} with a 1 cm^{-1} resolution using Bruker Vertex 70 spectrometer. The measurement time was ca. 5 min for each spectrum. Pure KBr in powdered form was used as a reference. Resulted spectra were transformed into absorption spectra using the Kubelka–Munk function.

The density functional theory: DFT calculations were performed using the Gaussian 16 program package [54] with the standard 6-311++G(d,p) basis set [55], including diffuse and polarization functions at all atoms. Ground-state geometry of complex (^{Me}imSQ)$_2$FeBr was optimized using the TPSSh meta-GGA [56] and B3LYP [57] exchange-correlation functionals. The stationary points on the potential energy surfaces (PESs) were located by full geometry optimization with the calculation of force constant matrices. Exchange coupling of unpaired electrons in the paramagnetic centers was estimated using the "broken symmetry" (BS) formalism [58].

Mössbauer spectroscopy: The Mössbauer spectra of (^{Me}imSQ)$_2$FeBr were measured by MS1104Em Mössbauer spectrometer in the temperature range 15-300 K. The sample was cooled in helium cryostat CCS-850 (Janis Res. Inc., USA). The ^{57}Co in rhodium matrix was used as a γ-ray source. The experimental spectra were fitted using SpectrRelax software [59]. The isomer shifts were calculated with respect to the metallic α-Fe.

Acknowledgements

This work is supported by the Russian Foundation for Basic Research (RFBR #18-02-40029). AAG, AAT and YVR acknowledge the President's Grant of Russian Federation for young scientists МК-2730.2019.2 (№ 075-15-2019-1099) for the financial support.

Keywords: Spin-crossover • valence-tautomerism • metal complexes • redox-active ligand • X-ray spectroscopy

[1] C.G. Pierpont, R.M. Buchanan, *Coord. Chem. Rev.* **1981**, *38*, 45-87.
[2] C.G. Pierpont, *Coord. Chem. Rev*. **2001**, *219*, 415-433.
[3] O. Sato, J. Tao, Y.Z. Zhang, *Ang. Chem. Int. Ed*. **2007**, *46*, 2152-2187.
[4] A.I. Poddel'sky, V.K. Cherkasov, G.A. Abakumov, *Coord. Chem. Rev*. **2009**, *253*, 291-324.
[5] P.J. Chirik, *Inorg. Chem*. **2011**, *50*, 9737-9740.
[6] M. Chegerev, A. Piskunov, *Russ. J. Coord. Chem*. **2018**, *44*, 258-271.
[7] W. Kaim, *Inorg. Chem*., **2011**, *50*, 9752-9765.
[8] R.M. Buchanan and C.G. Pierpont, *J. Am. Chem. Soc*. **1980**, *102*, 4951-4957.
[9] C.G. Pierpont, *Coord. Chem. Rev.* **2001**, *216*, 99-125.
[10] T. Tezgerevska, K.G. Alley, C. Boskovic, *Coord. Chem. Rev*. **2014**, *268*, 23-40.
[11] A. Bencini, A. Caneschi, C. Carbonera, A. Dei, D. Gatteschi, R. Righini, C. Sangregorio, J. Van Slageren, *J. Mol. Struct*. **2003**, *656*, 141-154.

[12] I.L. Fedushkin, O.V. Maslova, A.G. Morozov, S. Dechert, S. Demeshko, F. Meyer, *Ang. Chem. Int. Ed*. **2012**, *51*, 10584-10587.
[13] M.G. Chegerev, A.A. Starikova, A.V. Piskunov, V.K. Cherkasov, *Europ. J. Inorg. Chem*. **2016**, *2016*, 252-258.
[14] M.G. Chegerev, A.V. Piskunov, A.A. Starikova, S.P. Kubrin, G.K. Fukin, V.K. Cherkasov, G.A. Abakumov, *Europ. J. Inorg. Chem*. **2018**, *2018*, 1087-1092.
[15] A.A. Zolotukhin, M.P. Bubnov, A.V. Arapova, G.K. Fukin, R.V. Rumyantcev, A.S. Bogomyakov, A.V. Knyazev, V.K. Cherkasov, *Inorg. Chem*. **2017**, *56*, 14751-14754.
[16] C.W. Lange, M. Foldeaki, V. Nevodchikov, K. Cherkasov, G. Abakumov, C.G. Pierpont*, J. Am. Chem. Soc.* **1992**, *114***,** 4220-4222.
[17] O.-S. Jung, C.G. Pierpont*, J. Am. Chem. Soc.* **1994**, *116*, 2229-2230.
[18] H. Chun, T. Weyhermüller, E. Bill, K. Wieghardt, *Ang. Chem. Int. Ed.* **2001**, *40*, 2489-2492.
[19] H. Chun, E. Bill, T. Weyhermüller, K. Wieghardt, *Inorg. Chem*. **2003**, *42*, 5612-5620.
[20] A.V. Piskunov, K.I. Pashanova, I.V. Ershova, A.S. Bogomyakov, I.V. Smolyaninov, A.G. Starikov, S.P. Kubrin, G.K. Fukin, *J. Mol. Struct*. **2018**, *1165*, 51-61.
[21] S. Mukherjee, T. Weyhermüller, E. Bill, K. Wieghardt, P. Chaudhuri, *Inorg. Chem*. **2005**, *44,* 7099-7108.
[22] A.J. Simaan, M.L. Boillot, E. Rivière, A. Boussac, J.J. Girerd, *Ang. Chem*., **2000**, *112*, 202-204.
[23] S. Floquet, A. Simaan, E. Rivière, M. Nierlich, P. Thuéry, J. Ensling, P. Gütlich, J.-J. Girerd, M.-L. Boillot, *Dalton Trans*. **2005**, 1734-1742.
[24] A. Rajput, A.K. Sharma, S.K. Barman, D. Koley, M. Steinert, R. Mukherjee, *Inorg. Chem*. **2014***, 53*, 36-48.
[25] I.V. Ershova, A.V. Piskunov, V. K. Cherkasov, *Russ. Chem. Rev*. **2021**, *90* (in press).
[26] M. P. Bubnov, I. A. Teplova, K. A. Kozhanov, G. A. Abakumov, V. K. Cherkasov*, J. Magn. Reson.* **2011**, *209*, 149-155.
[27] K.A. Kozhanov, M.P. Bubnov, G.A. Abakumov, V.K. Cherkasov, *J. Magn. Reson.* **2012**, *225*, 62-70.
[28] M. P. Bubnov, K. A. Kozhanov, N. A. Skorodumova, I. A. Teplova, V. K. Cherkasov, A. V. Piskunov, E. V. Baranov, G. K. Fukin, A. S. Bogomyakov, *J. Mol. Struct*. **2019**, *1180*, 878-887.
[29] V. Lyaskovskyy, B. de Bruin, *Acs Catalysis* **2012**, *2*, 270-279.
[30] P.J. Chirik, K. Wieghardt, *Science* **2010**, *327*, 794-795.
[31] O.R. Luca, R.H. Crabtree, *Chem. Soc. Rev*. **2013**, *42*, 1440-1459.
[32] D.L. Broere, R. Plessius, J.I. van der Vlugt, *Chem. Soc. Rev*. **2015**, *44*, 6886-6915.
[33] L. Greb, F. Ebner, Y. Ginzburg and L. M. Sigmund, *Eur. J. Inorg. Chem*., 2020, 2020, 1.
[34] A. Caneschi, D. Gatteschi, P. Rey, *Prog. Inorg. Chem*. **1991**, 331-429.
[35] C.G. Pierpont, C.W. Lange, *Prog. Inorg. Chem*. **1994**, 331-442.
[36] W. Kaim, Dalton Trans. **2003**, 761-768.
[37] O. Sato, A. Cui, R. Matsuda, J. Tao, S. Hayami, *Acc. Chem. Res*. **2007,** *40*, 361-369.
[38] R.W. Hogue, S. Singh, S. Brooker, *Chem. Soc. Rev*., **2018**, *47*, 7303-7338.
[39] O. Kahn, C.J. Martinez, *Science* **1998**, *279*, 44-48.
[40] J. Miller, M. Drillon in *Magnetism: Molecules to Materials*, Willey, VCH: Weinheim, **2002**.
[41] D.N. Hendrickson, C.G. Pierpont in *Spin Crossover in Transition Metal Compounds II*, Springer, **2004**.
[42] M.A. Halcrow in *Spin-crossover materials: properties and applications*, John Wiley & Sons, **2013**.
[43] L. Credendino, S. Sproules, *Asian J. Org. Chem*. **2020**, *9*, 421–430.
[44] I.V. Ershova, A.S. Bogomyakov, S.P. Kubrin, G.K. Fukin, A.V. Piskunov, *Inorg. Chim. Acta* **2020**, *503*, 119402.
[45] G. Abakumov, V. Cherkasov, M. Bubnov, L. Abakumova, V. Ikorskii, G. Romanenko, A. Poddel'sky, *Russ. Chem. Bull*. **2006**, *55*, 44-52.
[46] A.M. Beale, M. Le, S. Hoste, G. Sankar, *Solid state sci.* **2005**, *7*, 1141-1148.
[47] F. Menil, *J. Phys. Chem. Solids* **1985**, *46*, 763-789.
[48] W.D. Federer, D.N. Hendrickson, *Inorg. Chem*. **1984**, *23*, 3861-3870.
[49] a) H. Funke, A. Scheinost, M. Chukalina, *Phys. Rev. B*, **2005**, *71*, 094110; b) H. Funke, M. Chukalina, A.C. Scheinost, *J. Synchrotron Rad*. **2007**, *14*, 426-432; c) A.S. Burlov, V.G. Vlasenko, Yu.V. Koshchienko, S.I. Levchenkov, I.V. Pankov, Ya.V. Zubavichus, A.L. Trigub, G.S. Borodkin, T.A. Mazepina, D.A. Garnovskii, A.I. Uraev, *Russ. J. Coord. Chem.* **2016**, *42*, 237-244.
[50] a) T.C. Berto, A.L. Speelman, S. Zheng, N. Lehnert, *Coord. Chem. Rev.* **2013**, *257*, 244 – 259; b) C.A. Brown, M.A. Pavlosky, T.E. Westre, Y. Zhang, B. Hedman, K. O.Hodgson, E.I. Solomon, *J. Am. Chem. Soc.* **1995**, *117*, 715–732; c) M. Li, D. Bonnet, E. Bill, F. Neese, T. Weyhermuller, N. Blum, D. Sellmann, K. Wieghardt, *Inorg. Chem.* **2002**, *41*, 3444–3456; d) T.C. Berto, M.B. Hoffman, Y. Murata, K.B. Landenberger, E.E. Alp, J. Zhao, N. Lehnert, *J. Am. Chem. Soc.* **2011**, *133*, 16714-16717; e) L. Piñeiro-López, N. Ortega-Villar, M. C. Muñoz, G. Molnár, J. Cirera, R. Moreno-Esparza, V. M. Ugalde-Saldívar, A. Bousseksou, E. Ruiz, J. A. Real, *Chem. Eur. J.* **2016**, *22*, 12741.
[51] B. Ravel and M. Newville, *J. Synchrotron Rad*. **2005**, *12*, 537-541.
[52] S. Zabinsky, J. Rehr, A. Ankudinov, R. Albers, M. Eller, *Phys. Rev. B,* **1995**, *52*, 2995-3009.
[53] S.A. Guda, A.A. Guda, M.A. Soldatov, K.A. Lomachenko, A.L. Bugaev, C. Lamberti, W. Gawelda, C. Bressler, G. Smolentsev, A.V. Soldatov, *J. Chem. Theor. Comp*. **2015**, *11*, 4512-4521.
[54] M.J. Frisch, G.W. Trucks, H.B. Schlegel, G.E. Scuseria, M.A. Robb, J.R. Cheeseman, G. Scalmani, V. Barone, G.A. Petersson, H. Nakatsuji, X. Li, M. Caricato, A.V. Marenich, J. Bloino, B.G. Janesko, R. Gomperts, B. Mennucci, H.P. Hratchian, J.V. Ortiz, A.F. Izmaylov, J.L. Sonnenberg, Williams, F. Ding, F. Lipparini, F. Egidi, J. Goings, B. Peng, A. Petrone, T. Henderson, D. Ranasinghe, V.G. Zakrzewski, J. Gao, N. Rega, G. Zheng, W. Liang, M. Hada, M. Ehara, K. Toyota, R. Fukuda, J. Hasegawa, M. Ishida, T. Nakajima, Y. Honda, O. Kitao, H. Nakai, T. Vreven, K. Throssell, J.A. Montgomery Jr., J.E. Peralta, F. Ogliaro, M.J. Bearpark, J.J. Heyd, E.N. Brothers, K.N. Kudin, V.N. Staroverov, T.A. Keith, R. Kobayashi, J. Normand, K. Raghavachari, A.P. Rendell, J.C. Burant, S.S. Iyengar, J. Tomasi, M. Cossi, J.M. Millam, M. Klene, C. Adamo, R. Cammi, J.W. Ochterski, R.L. Martin, K. Morokuma, O. Farkas, J.B. Foresman and D.J. Fox, *Gaussian 16* Rev. A.03, in, Wallingford, CT, **2016**.
[55] W.J. Hehre, R. Ditchfield and J.A. Pople, *J. Chem. Phys*. **1972**, *56*, 2257-2261.
[56] J. Tao, J.P. Perdew, V.N. Staroverov, G.E. Scuseria, *Phys. Rev. Lett*. **2003**, *91*, 146401.
[57] a) P.J. Stephens, F.J. Devlin, C.F. Chabalowski, M.J. Frisch, *J. Phys. Chem*. **1994**, *98*, 11623-11627; b) A.D. Becke, *J. Chem. Phys*. **1993**, *98*, 1372-1377.
[58] L. Noodleman, *J. Chem. Phys.* **1981**, *74*, 5737-5743.
[59] M. Matsnev, V. Rusakov, *AIP Conf. Proc., AIP*, **2012**, 178-185.

Entry for the Table of Contents

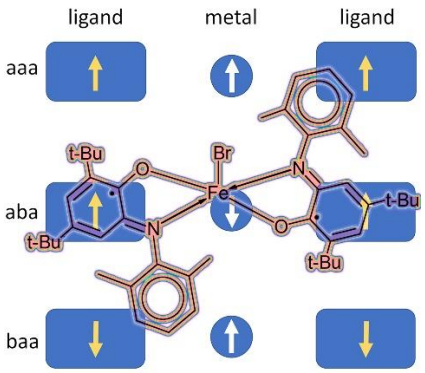

Unusual temperature-dependent magnetization in the pentacoordinate ferric bis-o-iminosemiquinonate complex is not related to the spin crossover. X-ray absorption spectroscopy quantified structural deformations originating from spin transition upon cooling. DFT simulations in broken symmetry approach explain these geometry changes by strong exchange interactions between spins on Fe and ligands.